Plasmon-enhanced spectral changes in surface sum-frequency generation with polychromatic light

Luyu Wang, Franklin Che, Sergey A. Ponomarenko*, and Zhizhang (David) Chen

Department of Electrical and Computer Engineering, Dalhousie University, Halifax, NS, B3J 2X4 Canada

*serpo@dal.ca

Abstract: We theoretically explore the spectral behavior of the fundamental and sum-frequency waves generated from the surface of a thin metal film in the Kretschmann configuration with coherent ultrashort pulses. We show that the spectra of reflected sum-frequency waves exhibit pronounced shifts for the incident fundamental waves close to the plasmon coupling angle. We also demonstrate that the scale of discovered plasmon-enhanced spectral changes is strongly influenced by the magnitude of the incidence angle and the bandwidth of the source spectrum.

OCIS codes: (240.6680) Surface plasmons; (300.6170) Spectra; (190.4350) Nonlinear optics at surfaces.

References and links

1. M. I. Stockman, "Nanoplasmonics: past, present, and glimpse into future," Opt. Express **19**, 22029–22106 (2011).
2. P. N. Prasad, *Nanophotonics* (Wiley, Hoboken, 2004).
3. L. Novotny and B. Hechi, *Principles of Nano-Optics* (Cambridge University, Cambridge, 2006).
4. L. M. Zhang and D. Uttamchandani, "Optical chemical sensing employing surface plasmon resonance," Electron. Lett. **23**, 1469–1470 (1988).
5. J. Homola, S. S. Yee, and G. Gauglitz, "Surface plasmon resonance sersors: review," Sensors and Actuators B **54**, 3–15 (1999).
6. H. J. Simon, D. E. Mitchell, and J. G. Watson, "Optical Second-Harmonic Generation with Surface Plasmons in Silver Films," Phys. Rev. Lett. **33**, 1531–1534 (1974).
7. A. Bouhelier, M. Beverslius, A. Hartschuh, and L. Novotny, "Near-field second-harmonic generation induced by local field enhancement," Phys. Rev. Lett. **90**, 13903–1–4 (2003).
8. S. I. Bozhevolny, J. Beermann, and V. Coello, "Direct observation of localized second-harmonic enhancement in random metal nanostructures," Phys. Rev. Lett. **90**, 197403–1–4 (2003).
9. M. Labardi, M. Allegrini, M. Zavelani-Rossi, D. Polli, G. Cerullo, S. D. Silvestri, and O. Sveto, "Highly efficient second-harmonic nanosource for near-field optics and microscopy," Opt. Lett. **29**, 62–64 (2004).
10. M. I. Stockman, D. G. Bergman, C. Anceau, S. Brasselet, and J. Zyss, "Enhanced second-harmonic generation by metal surfaces with nanoscale roughness: Nanoscale dephasing, depolarization, and correlations," Phys. Rev. Lett. **92**, 057402–1–4 (2004).
11. N. I. Zheludev and V. I. Emelyanov, "Phase-matched second harmonic generation from nanostructured metal surfaces," J. Opt. A. **6**, 26–28 (2004).
12. A. Liebsch, "Theory of sum frequency generation from metal surfaces," Appl. Phys. B **68**, 301–304 (1999).
13. E. M. M. van der Ham, Q. H. F. Vrehen, E. R. Eltel, V. A. Yakovlev, E. V. Alieva, L. A. Kuzik, J. E. Petrov, V. A. Sychugov, and A. F. G. van der Meer, "Giant enhancement of sum-frequency yeild by surface-plasmon excitation," J. Opt. Soc. Am. B **16**, 1146–1152 (1999).
14. A. T. Georges and N. E. Karatzas, "Optimizing the excitation of surface plasmon polaritions by difference-frequency generation on a gold surface," Phys. Rev. B **85**, 155442–1–5 (2012).

15. F. DeMartini, F. G. Giuliani, M. Mataloni, E. Palange, and Y. R. Shen, "Study of Surface Polaritons in GaP by Optical Four-Wave Mixing," Phys. Rev. Lett. **37**, 440–443 (1976).
16. S. Polomba and L. Novotny, "Nonlinear Excitation of Surface Plasmon Polaritons by Four-Wave Mixing," Phys. Rev. Lett. **101**, 056802–1–4 (2008).
17. R. M. Corn and D. A. Higgins, "Optical Second Harmonic Generation as a Probe of Surface Chemistry," Chem. Rev. **94**, 107–125 (1994).
18. J. Vydra and M. Eich, "Mapping of the lateral polar orientational distribution in second-order nonlinear thin films by scanning second-harmonic microscopy," Appl. Phys. Lett. **72**, 275–277 (1998).
19. T.-H. Lan, Y.-K. Chyng, J. Li, and C.-H. Tien, "Plasmonic rainbow rings induced by white radial polarization," Opt. Lett. **37**, 1205–1207 (2012).
20. Y. Nishijima, L. Roza, and S. Juodkazis, "Surface plasmon resonances in periodic and random patterns of gold nano-disks for broadband light harvesting," Opt. Express **20**, 11466–11477 (2012).
21. L. Mandel and E. Wolf, *Optical Coherence and Quantum Optics* (Cambridge University, Cambridge, 1995).
22. S. A. Ponomarenko, H. Roychowdhury, and E. Wolf, "Physical significance of complete spatial coherence of optical fields," Phys. Lett. A **345**, 10–12 (2005).
23. E. Kretschmann and H. Raether, "Radiative decay of non-radiative surface plasmons excited by light," Z. Naturforsch. A **23**, 2135–2136 (1968).
24. S. A. Ponomarenko, G. P. Agrawal, and E. Wolf, "Energy spectrum of nonstationary ensemble of pulses," Opt. Lett. **29**, 394–396 (2004).
25. W. C. Chew, *Waves and Fields in Inhomogeneous Media*, II ed. (Institute of Electrical and Electronics Engineers, New York, 1995).
26. R. W. Boyd, *Nonlinear Optics*, II ed. (Academic, Boston, 2003).
27. W. Hübner, K. H. Bennemann, and K. Böhmer, "Theory for the nonlinear optical response of transition metals: Polarization dependence as a fingerprint of the electronic structure at surfaces and interfaces," Phys. Rev. B **50**, 17597–17605 (1994).
28. F. X. Wang, F. J. Rodriguez, W. M. Albers, R. Ahorinta, J. E. Sipe, and M. Kauranen, "Surface and bulk contributions to the second-order nonlinear optical response of a gold film," Phys. Rev. B **80**, 233402–1–4 (2009).
29. D. Krause, C. W. Teplin, and C. T. Rogers, "Optical surface second harmonic measurements of isotropic thin-film metals: Gold, silver, copper, aluminum, and tantalum," J. Appl. Phys. **96**, 3626–3634 (2004).
30. J.-C. Diels and W. Rudolph, *Ultrashort Laser Pulse Phenomena*, II ed. (Academic, Boston, 2006).
31. J. A. Maytorena, W. L. Mochán, and B. S. Mendoza, "Hydrodynamic model of sum and difference frequency generation at metal surfaces," Phys. Rev. B **57**, 2580-2585 (1998).
32. S. A. Ponomarenko and E. Wolf, "Spectral anomalies in Fraunhofer diffraction," Opt. Lett. **27**, 1211–1213 (2002).

1. Introduction

The field of plasmonics has lately experienced a truly explosive growth [1]. Much research in plasmonics has so far been focused on linear light-matter interaction modalities [2, 3], owning largely to the success of plasmonic-based sensors as a powerful tool for probing surfaces [4, 5]. However, resonantly enhanced local electric fields bring about pronounced enhancement of nonlinear responses of plasmonic materials as well [1]. To date, several plasmon-enhanced nonlinear optical phenomena have been explored, including second-harmonic generation (SHG) from deterministic [6, 7], random [8–10], and phase-matched [11] nanostructured surfaces. While SHG can be realized with a quasi-monochromatic light source of a fundamental wave (FW), the sum-frequency generation (SFG) [12, 13] or difference-frequency generation (DFG) [14] in plasmonic materials is more difficult to realize experimentally; this is because it requires two such sources with distinct carrier frequencies as, in general, does surface plasmon excitation by four-wave mixing [15, 16]. These second- and third-order nonlinear processes are surface sensitive at the molecular level, rendering them highly attractive for nonlinear microscopy. In fact, one such modality, the second-harmonic microscopy, has already been proposed and studied [17, 18].

Although the vast majority of work in plasmonics deals with quasi-monochromatic light, there has been growing interest in spectral signatures of plasmon enhanced electromagnetic fields. In particular, the *linear* optical response of homogenous [19] and inhomogeneous–periodic or random [20]–plasmonic nanostructures, probed with broadband light beams, has

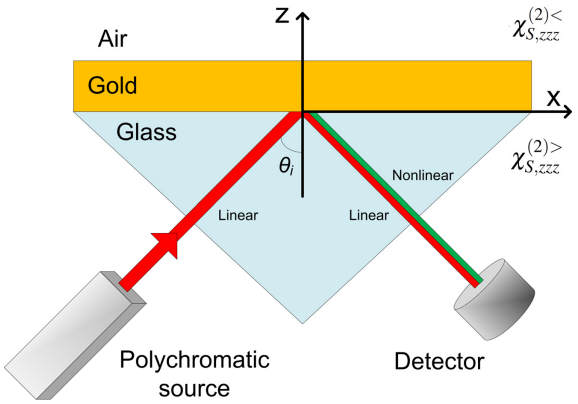

Fig. 1. Illustrating the Kretschmann configuration.

been recently examined. However, to the best of our knowledge, plasmon-enhanced *nonlinear* optical processes, excited by polychromatic light sources, have not yet been studied. In this context, it is especially instructive to learn whether plasmons, excited on the surface of a conducting material or nanostructure, leave any signatures in the far-field spectra of generated second-order nonlinear waves. The affirmative answer to this question can trigger new developments in surface nonlinear spectroscopy, microscopy, and surface morphology studies.

In this work, we investigate the spectral behavior of the fundamental and sum-frequency waves in the surface SFG from a thin metal film with the polychromatic incident light. We assume that the source field is well collimated such that it can be treated as a plane wave. The wide bandwidth of the source makes it possible to realize SFG with a single source: any pair of monochromatic components within the source spectrum gives rise to a sum-frequency component through the surface SFG process. For symmetric source spectra, one would expect the SFG spectrum to peak at half the carrier wavelength of the source. We show, however, that at the incidence angle corresponding to light coupling to the surface plasmon, the reflected sum-frequency wave (SFW) spectrum gets blue-shifted from the expected maximum whereas the reflected FW has a spectral hole at the carrier frequency. We further demonstrate that the magnitude of the effect depends on the bandwidth of the source spectrum and the incidence angle: the shifts of SFW spectra become more pronounced as the source bandwidth increases, while at a certain angle a spectral switch is observed. Also, as the incidence angle deviates from the plasmon coupling angle, all spectral changes disappear. The appearance of large SFW shifts can serve as an unambiguous plasmon signature in nonlinear surface spectroscopy.

2. Theory

We consider fully spatially coherent incident light [21, 22], which we assume to behave as a plane wave. We examine the spectral behavior of fundamental and sum-frequency waves in the Kretschmann geometry [23] illustrated in Fig. 1. A thin metal (gold) film is illuminated by a *p*-polarized polychromatic plane wave from glass ($\varepsilon_1 = 2.25$) at the angle of incidence θ_i. The gold film has a thickness d and relative dielectric permittivity $\varepsilon_2(\omega)$. The incident wave with the spectral amplitude $A(\omega)$ can be represented as

$$\mathbf{E}_i(x,z,\omega,\theta_i) = A(\omega)\left(\frac{k_{1z}}{k_1}\mathbf{e}_x - \frac{k_x}{k_1}\mathbf{e}_z\right)e^{i(k_x x + k_{1z} z)}, \tag{1}$$

where $\mathbf{k}_1 = (k_x, 0, k_{1z})$ and $k_1 = \omega\sqrt{\mu_0\varepsilon_1}$; $\mathbf{e}_x$ and $\mathbf{e}_z$ are unit vectors in the x- and z-directions, respectively. The components of the wave vector $\mathbf{k}_1$ can be expressed as $k_x = k_1 \sin\theta_i$ and $k_{1z} = k_1 \cos\theta_i$. The finite bandwidth of the incident light can originate either from partial temporal coherence or from a pulsed nature of the source. We assume henceforth that the incident light wave is produced by a coherent femtosecond laser source which provides sufficiently large input intensities to generate a nonlinear optical response of the system. Thus, we introduce the energy spectrum of the incident pulse by the expression [24]

$$S_i(\omega) \propto |\mathbf{E}_i(x,z,\omega,\theta_i)|^2 = |A(\omega)|^2, \tag{2}$$

up to an immaterial proportionality constant.

The (multiply) reflected FW strikes the detector. Using the standard multiple-reflection Airy method it can be inferred that the reflected wave is

$$E_r(x,z,\omega,\theta_i) = A(\omega)\left(-\frac{k_{1z}}{k_1}\mathbf{e}_x - \frac{k_x}{k_1}\mathbf{e}_z\right)\tilde{r}_{12}(\omega,\theta_i)e^{i(k_x x - k_{1z} z)}. \tag{3}$$

The reflected energy spectrum can then be written as

$$S^{(1)}(\omega,\theta_i) \propto |\mathbf{E}_r(x,z,\omega,\theta_i)|^2 \propto |\tilde{r}_{12}(\omega,\theta_i)|^2 S_i(\omega). \tag{4}$$

Here $\tilde{r}_{12}(\omega,\theta_i)$ is the double-interface Fresnel reflection coefficient for p-polarization given by [25]

$$\tilde{r}_{12}(\omega,\theta_i) = \frac{r_{12} + r_{23}e^{i2k_{2z}d}}{1 + r_{12}r_{23}e^{i2k_{2z}d}}, \tag{5}$$

where $k_{2z} = \sqrt{k_2^2 - k_x^2}$.

Next, the FW gives rise to nonlinear polarizations on both interfaces of the film. In general, the i'th component ($i = x, y,$ or z) of the sum-frequency polarization field can be written as [26]

$$P_i(\mathbf{r},\omega_3) = \varepsilon_0 \sum_{jk} \int_{-\infty}^{\infty} \frac{d\omega_1}{2\pi} \chi^{(2)}_{ijk}(-\omega_3;\omega_1,\omega_2) E_j(\mathbf{r},\omega_1) E_k(\mathbf{r},\omega_2), \tag{6}$$

where ω_1 and ω_2 are pump frequencies while $\omega_3 = \omega_1 + \omega_2$ represents the generated nonlinear frequency, and $\mathbf{r} = (x,y,z)$; $\chi^{(2)}_{ijk}(-\omega_3;\omega_1,\omega_2)$ is the nonlinear susceptibility tensor of the sum-frequency generation (SFG) process. The subscripts denote the Cartesian field components tangential and normal to the interface, respectively. It was argued theoretically [27] that at relatively large pump wavelengths ($\lambda \geq 690$ nm for gold), the leading contribution to the nonlinear polarization comes from the diagonal surface component $\chi^{(2)}_{S,zzz}$ of the second-order susceptibility tensor. This claim is supported with the available SHG experimental data [28,29], and it has been recently employed in a surface DFG study [14]. Hence, we will ignore the other contributions to $\chi^{(2)}$ hereafter. Therefore, we will only need the z-component of the field at the top and bottom of the film to determine the polarization fields in Eq. (6).

It can be shown that the total FW field in the glass is simply a superposition of the incident and reflected waves in Eqs. (1) and (3), respectively. The normal component of the reflected electric field is then

$$E_{1z}(x,z,\omega,\theta_i) = -\frac{k_x}{k_1} A(\omega) e^{ik_x x}\left[e^{ik_{1z}z} + \tilde{r}_{12}(\omega,\theta_i)e^{-ik_{1z}z}\right]. \tag{7}$$

The field on the lower interface can be found by taking $z = 0$. In addition, on applying the boundary condition for the normal components of the field on both sides of the lower interface, we obtain the field on the metal side of the lower interface as

$$E^{<}_{2z}(x,\omega,\theta_i) = -\frac{k_x}{k_1}\frac{\varepsilon_1}{\varepsilon_2} A(\omega) e^{ik_x x}\left[1 + \tilde{r}_{12}(\omega,\theta_i)\right]. \tag{8}$$

Similarly, the total FW field in the film is a superposition of the waves transmitted and reflected by the upper interface. The corresponding normal component of the field can be represented as

$$E_{2z}(x,z,\omega,\theta_i) = -\frac{k_x}{k_2}A(\omega)e^{ik_x x}\frac{t_{12}}{1+r_{12}r_{23}e^{i2k_{2z}d}}\left[e^{ik_{2z}z}+r_{23}e^{i2k_{2z}d}e^{-ik_{2z}z}\right]. \tag{9}$$

At the upper interface $z=d$, we have

$$E_{2z}^{>}(x,\omega,\theta_i) = -\frac{k_x}{k_2}A(\omega)e^{ik_x x}R(\omega,\theta_i), \tag{10}$$

where

$$R(\omega,\theta_i) = \frac{t_{12}(1+r_{23})e^{ik_{2z}d}}{1+r_{12}r_{23}e^{i2k_{2z}d}}. \tag{11}$$

On substituting from Eqs. (8) and (10) into Eq. (6), the polarization fields at the upper and lower interfaces read

$$\mathbf{P}^{<}(x,\omega_3,\theta_i) = \mathbf{e}_z P_0^{<}(\omega_3,\theta_i)e^{ik_x(\omega_3)x}, \tag{12}$$

$$\mathbf{P}^{>}(x,\omega_3,\theta_i) = \mathbf{e}_z P_0^{>}(\omega_3,\theta_i)e^{ik_x(\omega_3)x}, \tag{13}$$

where $k_x(\omega_3) = k_1(\omega_3)\sin\theta_i$, $k_1(\omega_3) = \omega_3\sqrt{\mu_0\varepsilon_1}$, and we introduced

$$\begin{aligned} P_0^{<}(\omega_3,\theta_i) =& \varepsilon_0\varepsilon_1^2\sin^2\theta_i\int_{-\infty}^{\infty}\frac{d\omega_1}{2\pi}\chi_{S,zzz}^{(2)<}(-\omega_3;\omega_1,\omega_2) \\ &\times\frac{A(\omega_1)A(\omega_2)}{\varepsilon_2(\omega_1)\varepsilon_2(\omega_2)}\left[1+\tilde{r}_{12}(\omega_1,\theta_i)\right]\left[1+\tilde{r}_{12}(\omega_2,\theta_i)\right], \end{aligned} \tag{14}$$

and

$$\begin{aligned} P_0^{>}(\omega_3,\theta_i) =& \varepsilon_0\varepsilon_1\sin^2\theta_i\int_{-\infty}^{\infty}\frac{d\omega_1}{2\pi}\chi_{S,zzz}^{(2)>}(-\omega_3;\omega_1,\omega_2) \\ &\times\frac{A(\omega_1)A(\omega_2)}{\sqrt{\varepsilon_2(\omega_1)\,\varepsilon_2(\omega_2)}}R(\omega_1,\theta_i)R(\omega_2,\theta_i). \end{aligned} \tag{15}$$

These polarizations act as the sources of secondary upconverted SFW. The i'th Cartesian component of the resulting sum-frequency field is determined from Maxwell's equations to be

$$E_i(r,\omega) = \frac{(\omega/c)^2}{\varepsilon_0}\sum_j\int d\mathbf{r}'G_{ij}(\mathbf{r},\mathbf{r}',\omega)P_j(\mathbf{r}',\omega). \tag{16}$$

Here $G_{ij}(\mathbf{r},\mathbf{r}',\omega)$ is the dyadic Green's tensor which can be expressed as [3]

$$G_{ij}(\mathbf{r},\mathbf{r}',\omega) = \left[\delta_{ij}+\frac{1}{k^2}\nabla_i\nabla_j\right]G_0(\mathbf{r},\mathbf{r}',\omega), \tag{17}$$

where $G_0(\mathbf{r},\mathbf{r}',\omega)$ is the scalar free-space Green's function representing an outgoing spherical wave from a point source. We use the Weyl identity to expand the spherical wave into an angular spectrum of plane waves [3, 21]

$$G_0(\mathbf{r},\mathbf{r}',\omega) = \frac{e^{ik|\mathbf{r}-\mathbf{r}'|}}{4\pi|\mathbf{r}-\mathbf{r}'|} = \frac{i}{8\pi^2}\int_{-\infty}^{\infty}\frac{dk_x}{k_z}e^{ik_x(x-x')+ik_z(z-z')}. \tag{18}$$

Note that the problem we study is two-dimensional implying that $\mathbf{r}=(x,0,z)$ and $\mathbf{r}'=(x',0,z')$. The nonlinear polarization field at the lower interface $\mathbf{P}^{<}$ gives rise to a contribution to the SFW

through the field directly reflected into the lower half-space. It can be obtained by substituting from Eqs. (12) and (17) into Eq. (16), and using Eq. (18), yielding

$$\mathbf{E}^{(2)<}_{down}(x,z,\omega_3,\theta_i) = \frac{i\omega_3 \sin\theta_i}{8\pi^2\varepsilon_0 c\sqrt{\varepsilon_1}} P_0^{<}(\omega_3,\theta_i)(-\mathbf{e}_x + \tan\theta_i \mathbf{e}_z) e^{i[k_x(\omega_3)x - k_{1z}(\omega_3)z]}, \tag{19}$$

where $\mathbf{k}_1(\omega_3) = k_x(\omega_3)\mathbf{e}_x + k_{1z}(\omega_3)\mathbf{e}_z$. By the same token, the other contribution from $\mathbf{P}^{<}$ to the SF field, partially transmitted into the film and eventually reflected back to the lower half-space, is

$$\begin{aligned}\mathbf{E}^{(2)<}_{up}(x,z,\omega_3,\theta_i) =& \frac{i\omega_3 \sin\theta_i}{8\pi^2\varepsilon_0 c\sqrt{\varepsilon_2(\omega_3)}} P_0^{<}(\omega_3,\theta_i)(-\mathbf{e}_x + \tan\theta_i \mathbf{e}_z) \\ &\times \frac{r_{23}t_{21}e^{i2k_{2z}(\omega_3)d}}{1 + r_{12}r_{23}e^{i2k_{2z}(\omega_3)d}} e^{i[k_x(\omega_3)x - k_{1z}(\omega_3)z]}.\end{aligned} \tag{20}$$

The Fresnel coefficients here are all evaluated at the frequency $\omega_3 = \omega_1 + \omega_2$ while $k_2(\omega_3) = \sqrt{k_x^2(\omega_3) + k_{2z}^2(\omega_3)}$.

The contribution to the reflected SFW from the nonlinear polarization field at the upper interface $\mathbf{P}^{>}$ is determined as

$$\begin{aligned}\mathbf{E}^{(2)>}(x,z,\omega_3,\theta_i) =& \frac{i\omega_3 \sin\theta_i}{8\pi^2\varepsilon_0 c\sqrt{\varepsilon_2(\omega_3)}} P_0^{>}(\omega_3,\theta_i)(-\mathbf{e}_x + \tan\theta_i \mathbf{e}_z) \\ &\times \frac{t_{21}e^{i2k_{2z}(\omega_3)d}}{1 + r_{12}r_{23}e^{i2k_{2z,\omega_3}d}} e^{i[k_x(\omega_3)x - k_{1z}(\omega_3)z]}.\end{aligned} \tag{21}$$

Finally, combining Eqs. (19)–(21), the energy spectrum of the reflected SFW in the lower half-space is found to be

$$S^{(2)}(\omega_3,\theta_i) \propto \left|\mathbf{E}^{(2)<}_{down}(x,z,\omega_3,\theta_i) + \mathbf{E}^{(2)<}_{up}(x,z,\omega_3,\theta_i) + \mathbf{E}^{(2)>}(x,z,\omega_3,\theta_i)\right|^2. \tag{22}$$

3. Results

We utilize Eqs. (4) and (22) to evaluate the spectra of FW and SFW at the detector. The laser source is assumed to be tunable, generating ultrashort pulses of duration ranging from 30 to 90 fs (FWHM). This translates to the bandwidth of approximately 3.33×10^{13} to 1.0×10^{14} s^{-1} assuming a Gaussian pulse profile; typical Ti-sapphire lasers generate femtosecond pulses in this temporal range [30]. The carrier wavelength of the source spectrum is assumed to be λ_0 = 1162 nm. The gold film has a thickness of d = 50 nm. To describe linear dielectric properties of the film, we employ a modified Drude-Sommerfeld model which takes into account the contributions from free and bound (interband transitions) electrons resulting in [3]

$$\varepsilon_2(\omega) = 1 - \frac{\omega_p^2}{\omega^2 + i\Gamma\omega} + \frac{\tilde{\omega}_p^2}{\omega_0^2 - \omega^2 - i\gamma\omega}. \tag{23}$$

The parameters of the model are: plasma frequencies, $\omega_p = 13.8\times10^{15}s^{-1}$ and $\tilde{\omega}_p = 4.5\times10^{15}s^{-1}$; damping rates, $\Gamma = 1.075\times10^{15}s^{-1}$ and $\gamma = 9\times10^{14}s^{-1}$; bound electron resonant frequency, $\omega_0 = 4.187\times10^{15}s^{-1}$. The surface nonlinear susceptibility is described within the framework of a hydrodynamic model developed in [31]. The leading contribution reads

$$\chi^{(2)}_{S,zzz}(-\omega_3;\omega_1,\omega_2) = -\frac{a(\omega_1,\omega_2)\,[\varepsilon_2(\omega_1)-1]\,[\varepsilon_2(\omega_2)-1]}{32\pi^2 n_B e}, \tag{24}$$

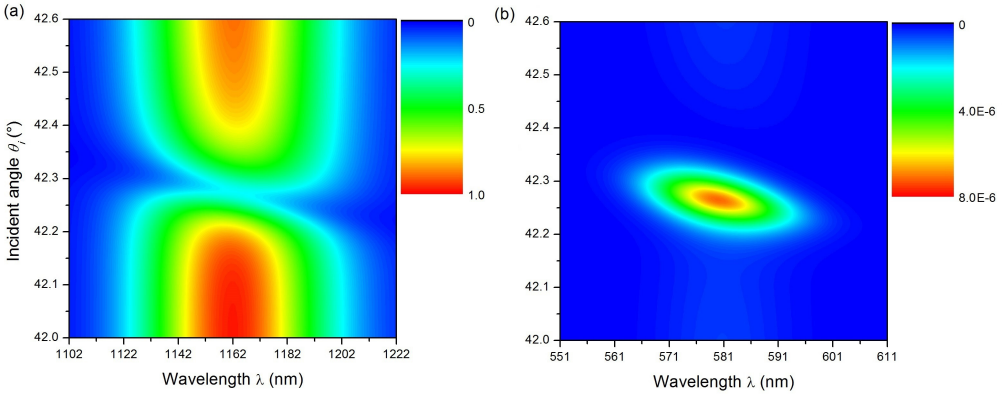

Fig. 2. Far-field energy spectra of (a) FW and (b) SFW around the plasmon coupling angle. The source pulse duration is $t_p = 90$ fs.

where n_B is the equilibrium free-electron density in the bulk. The dimensionless parameter $a(\omega_1, \omega_2)$ is essentially frequency-independent whenever the two pump frequencies ω_1 and ω_2 lie well below the volume plasma frequency ω_p. In our case, $\Delta\omega < 0.1\omega_0$ and $\omega_0/\omega_p \approx 0.117$, implying that any frequency within the source bandwidth is much smaller than ω_p. Hence, we may safely treat $a(\omega_1, \omega_2)$ as a constant. The evaluated $\chi^{(2)}_{S,zzz}(-\omega_3; \omega_1, \omega_2)$ is then of the order of 10^{-18} m^2/V (10^{-12} cm^2/statvolt in Gaussian units), showing excellent agreement with the experimental results of [29].

The plasmon coupling angle is given by [3]

$$\theta_c(\omega) = \sin^{-1}\sqrt{\frac{\varepsilon_2(\omega)}{\varepsilon_1\left[\varepsilon_2(\omega)+1\right]}}. \tag{25}$$

In our case, $\theta_c(\omega_0) \approx 42.3^\circ$. Under these conditions, free electrons in the film respond collectively to incident light waves by oscillating in resonance with the FW, i.e., surface plasmon resonance (SPR) occurs. It can be clearly seen in Fig. 2(a) that due to the efficient coupling to surface plasmons, the reflected FW has a hole in the far-field spectrum. The electromagnetic energy is localized near the film-air interface, dramatically enhancing the efficiency of SFG. The generated SFW is then reflected from the glass back to the detector and a large spectral peak, clearly visible in Fig. 2(b), is registered. Notice that the SFW is much better localized than the FW. For symmetric source spectra, one would expect the SFW spectrum to have a maximum at half the carrier wavelength of the FW (581 nm). However, the peak is actually blue-shifted with respect to the expected position. We conclude that the SPR leaves unambiguous signatures in the far-field spectrum of generated SFW.

To better illustrate spectral aspects of SFG in the system, we normalize the SFW spectrum of Fig. 2(b) to the corresponding maximum value for each θ_i and display the result in Fig. 3. In Fig. 3(a), we exhibited the SFW spectrum in a narrow range of incidence angles around the plasmon coupling angle. It can be inferred from the figure that the SPR gives rises to an overall blue-shift of the SFW spectrum. Displaying a wider incidence angle range in Fig. 3(b), we can observe that there is another (smaller) spectral shift toward the blue around 46°. This results from the SPR at SFW wavelengths: as long as the SFW is generated due to the strong FW enhancement, it can also be coupled to surface plasmons resulting in SPR excitation in the SFW. The corresponding plasmon coupling angle can be determined from the equation identical

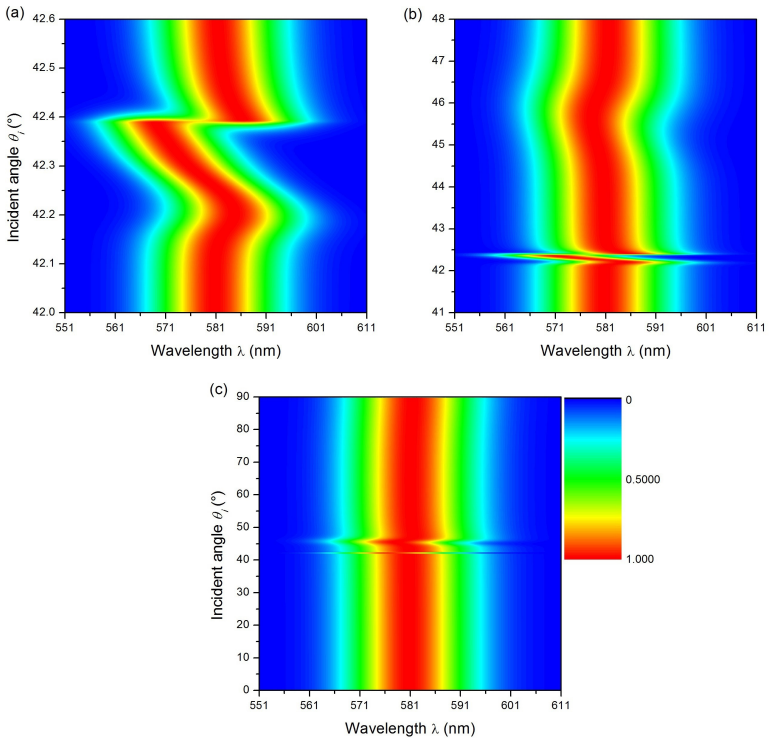

Fig. 3. Normalized far-field SFW energy spectrum for different incident angle ranges. The source pulse duration is $t_p = 90$ fs.

to Eq. (25), except ε_2 is evaluated at $2\omega_0$ leading to $\theta_c^{(2)}(2\omega_0) \approx 45.6^\circ$. As is seen in Fig. 3(c), which shows the SFW spectrum on an even larger scale, the spectrum is consistently centered at 581 nm for incidence angles ranging from 0 to 90°, except in the neighborhood of linear and nonlinear SPRs. As the incidence angle deviates a little from θ_c or $\theta_c^{(2)}$, the magnitude of the corresponding spectral shift falls off precipitously.

We can also show that the magnitude of discovered spectral changes is strongly influenced by the bandwidth of the source spectrum. To drive this point home, we display in Fig. 4 relative shifts of the mean fundamental (sum-frequency) wavelength relative to the (half) pump carrier wavelength as functions of the incidence angle for different pulse durations. It can be inferred from the figure that the shorter the pulse duration, the larger the spectral shift. More specifically, as we increase the source bandwidth, a sharp transition from blue to red in the vicinity of the plasmon coupling angle, seen in Fig. 3(a), transforms to a spectral dip. We observe such a spectral switch in Fig. 5(a) at $\theta_i = 42.47^\circ$ for the input pulse of $t_p = 30$ fs duration. Qualitatively, the present spectral switch is similar to the one previously discovered in Fraunhofer diffraction of light by a circular aperture [32]. We note that for the incidence angles outside the immediate neighborhood of the switch angle, the SFW spectrum displays no anomalous features, remaining Gaussian-like. We stress that the appearance of extremely surface-sensitive features in the reflected SFW spectrum can provide for environmental sensing with unprecedented accuracy. Indeed, any tiny perturbation of the film surface, leading to the corresponding change in the refractive index, can cause a switch of the SFW spectrum. Although the principle has been previously employed in conventional *linear* plasmonic sensor configurations [3–5], the use of

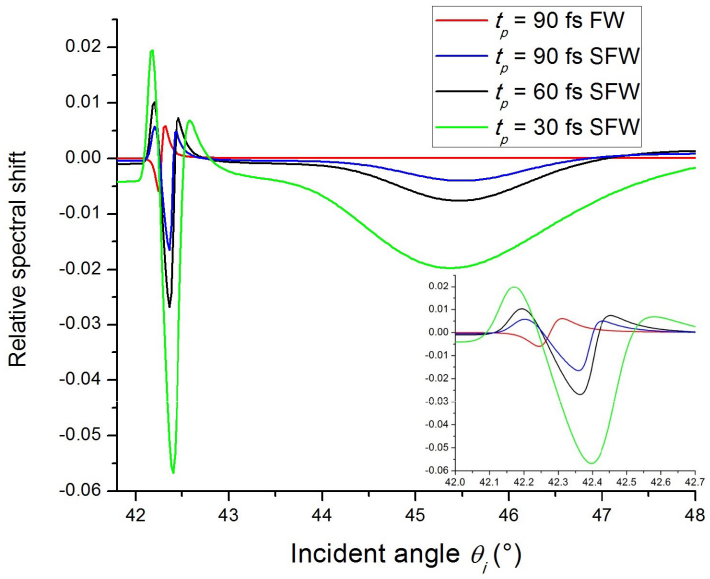

Fig. 4. Relative shifts of mean fundamental (sum-frequency) wavelengths at different incident angles with respect to the (half) pump carrier wavelength for different source pulse durations. Insert shows relative spectral shifts for incidence angles in the vicinity of the plasmon coupling angle. Negative values indicate blue shifts.

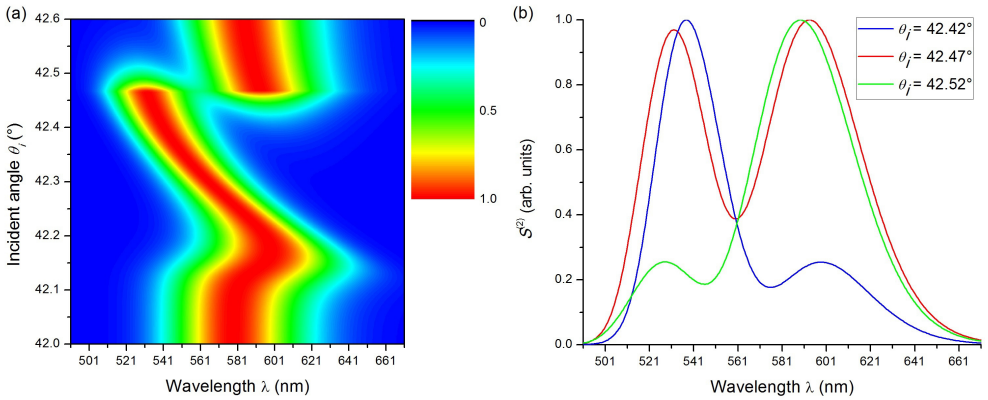

Fig. 5. (a) Normalized far-field SFW energy spectrum in the vicinity of the plasmon coupling angle with an incident pulse duration of t_p = 30 fs. (b) The SFW spectral switch.

nonlinear wave spectra can help attain, perhaps, a single-atom level of accuracy. This point is illustrated in Fig. 5(b) where we show that the SFW spectral behavior at the switch angle is sensitive to the angle variations of just a fraction of a degree.

4. Summary

To summarize, we theoretically explored the spectral behavior of surface-enhanced sum-frequency generation from a thin metal film produced with coherent ultrashort laser pulses.

We have shown that while spectra of fundamental waves, reflected at the angle corresponding to surface plasmon excitation in the film, can have a hole at the carrier freqency, the resonantly enhanced sum-frequency waves display pronounced spectral shifts. Thus, excited surface plasmons leave characteristic signatures in the spectra of fundamental and sum-frequency waves. We have also revealed that the discovered spectral changes strongly depend on the incidence angle and the bandwidth of the source spectrum, as well as observed a spectral switch which is sensitive to the angle variations. Our results may open up new avenues in nonlinear spectroscopy, surface plasmon sensing, and surface morphology studies.